ELSEVIER

Optics and Lasers in Engineering 26 (1997) 437–447

0143-8166/97/$15·00

0143-8166(95)00142-5

Fringe Formation in Symmetric Three-aperture Speckle Shear Interferometry: an Analysis

N. Krishna Mohan & R. S. Sirohi

Applied Optics Laboratory, Department of Physics, Indian Institute of Technology, Madras 600 036, India

(Received 30 August 1994; revised version received and accepted 15 March 1995)

ABSTRACT

Multi-aperture speckle shear interferometry also exhibits sensitivity to the in-plane displacement component. The interferogram obtained even at normal illumination contains fringes due to the combined contributions of slope, strain and in-plane components. The fringe pattern, therefore, changes when the shear element is placed at different aperture positions for the same experimental conditions. We have examined a three-aperture symmetric configuration where the shear element is either placed at the peripheral aperture or at the central aperture. The experimental results are presented. Copyright © 1996 *Elsevier Science Ltd.*

1 INTRODUCTION

Speckle interferometry is a suitable tool for the measurement of displacement components, while speckle shear interferometry is used to measure the spatial derivatives of the displacement components[1] and also of the wavefront.[2] In speckle shear interferometry, the contributions from two or more neighbouring points on the object are imaged on a single point. Alternatively a single object point is imaged as two or more points. This can be accomplished using a shear element in front of the imaging lens. The imaging lens carries a shear element either on its half-aperture[3] or on an aperture in a multi-aperture mask in front of it.[4,5] The multi-aperture configurations are intrinsically in-plane displacement sensitive, i.e. the derivative fringes will have in-plane displacement contributions and hence one should use these multi-aperture speckle shear interferometers with extreme caution.[6–8] It has also been shown recently that the in-plane displacement contribution can be separated from the combined patterns

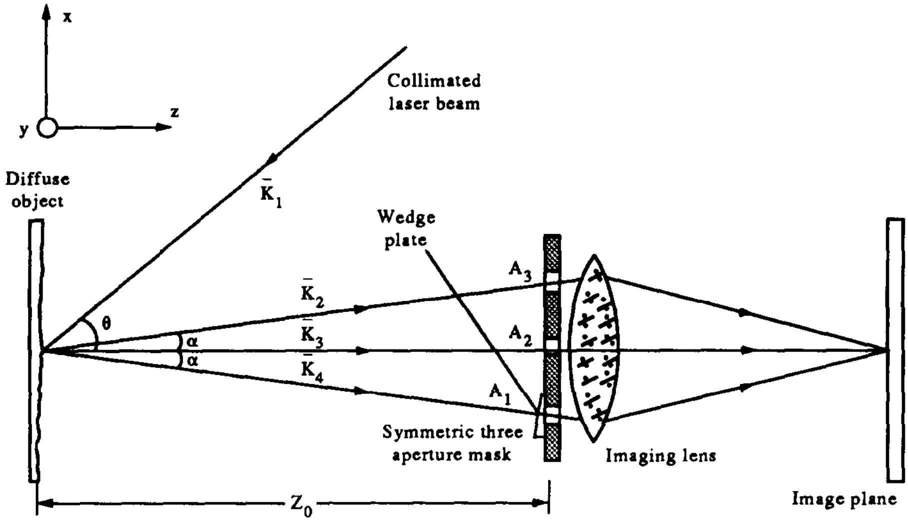

Fig. 1. Schematic of a symmetric three-aperture speckle shear interferometric arrangement.

to obtain slope distribution.[9] In this paper we present a detailed analysis of fringe formation in the presence of an in-plane displacement contribution with respect to location of a shear element in a symmetrical three-aperture configuration. Both theory and experimental results are presented.

2 SYMMETRICAL THREE-APERTURE CONFIGURATION WITH A SHEAR ELEMENT ON APERTURE A_1

The experimental arrangement is shown in Fig. 1. The imaging lens carries a mask containing three equi-spaced apertures along the x direction. Aperture A_1 carries a wedge plate which is the shear element. The object is illuminated with a collimated laser beam. The object plane shear, Δx_o, is $z_o(\mu_o - 1)\alpha_o$, where μ_o and α_o are the refractive index and the refracting angle of the wedge plate and z_o is the object distance measured from the wedge plate. The image plane shear, Δx, is $(\Delta x_o)M$, where M is the magnification of the imaging lens.

The amplitude distribution at any point on the image plane can be written as a sum of fields passing through the three apertures, i.e.

$$B_1 = a_1 \exp i(\phi_1 - \beta) + a_2 \exp i(\phi_2) + a_3 \exp i(\phi_3 + \beta) \tag{1}$$

where as and ϕs are the amplitudes and phases of the waves and $\beta = 2\pi\mu x$ is the phase introduced between the waves by the aperture separation, and is responsible for the grating-like structure in each speckle. The contribution at the image point via aperture A_1 arrives from a point that is sheared by Δx_o along the x direction.

The irradiance distribution on the image plane is obtained by

$$I_1 = B_1 B_1^* = |a_1|^2 + |a_2|^2 + |a_3|^2 + 2a_1a_2 \cos(\phi_{12} + \beta) + 2a_2a_3 \cos(\phi_{23} + \beta) + 2a_1a_3 \cos(\phi_{13} + 2\beta) \quad (2)$$

where $\phi_{12} = \phi_1 - \phi_2$, $\phi_{23} = \phi_2 - \phi_3$ and $\phi_{13} = \phi_1 - \phi_3$.

When the object is deformed, the phases of the waves via the three apertures change. The amplitude at the same point after object deformation can be expressed as

$$B_2 = a_1 \exp i(\phi_1 - \beta + \delta_1) + a_2 \exp i(\phi_2 + \delta_2) + a_3 \exp i(\phi_3 + \beta + \delta_3) \quad (3)$$

where δ_1, δ_2 and δ_3 are the phase changes introduced by deformation. The phases can be expressed in terms of directions of observation and directions of illumination, and are given by

$$\begin{aligned} \delta_1 &= (\mathbf{K}_4 - \mathbf{K}_1) \cdot \mathbf{L}(x + \Delta x_o, y) \\ \delta_2 &= (\mathbf{K}_3 - \mathbf{K}_1) \cdot \mathbf{L}(x, y) \\ \delta_3 &= (\mathbf{K}_2 - \mathbf{K}_1) \cdot \mathbf{L}(x, y) \end{aligned} \quad (4)$$

where $\mathbf{K}_1$ is the propagation vector along the illumination direction; $\mathbf{K}_2$, $\mathbf{K}_3$, $\mathbf{K}_4$ are the propagation vectors along the directions of observation; and $\mathbf{L}(x, y)$ and $\mathbf{L}(x + \Delta x_o, y)$ are the deformation vectors at the two points (x, y) and $(x + \Delta x_o, y)$, respectively. The components of deformation vectors at these points are (u, v, w) and $(u + \Delta u, v + \Delta v, w + \Delta w)$, respectively.

The irradiance distribution at the image plane after deformation is given as

$$I_2 = B_2 B_2^* = |a_1|^2 + |a_2|^2 + |a_3|^2 + 2a_1a_2 \cos(\phi_{12} + \beta + \delta_{12}) + 2a_2a_3 \cos(\phi_{23} + \beta + \delta_{23}) + 2a_1a_3 \cos(\phi_{13} + 2\beta + \delta_{13}) \quad (5)$$

where $\delta_{12} = \delta_1 - \delta_2$, $\delta_{23} = \delta_2 - \delta_3$ and $\delta_{13} = \delta_1 - \delta_3$.

The irradiance distributions I_1 and I_2 are sequentially recorded on the same photographic plate. Assuming linear recording, the amplitude transmittance $t(x, y)$ of the specklegram is given as

$$t(x, y) = t_o - \beta_o T(I_1 + I_2) \quad (6)$$

where β_o is constant and T is the exposure time for each recording.

When such a specklegram is placed in whole-field filtering arrangement as shown in Fig. 2, five haloes are formed including the zeroth order at the focal plane of lens L_1. The first-order haloes arise due to the superposition of fourth and fifth terms of eqns (2) and (5), while the second-order haloes are due to the sixth term from these equations. Filtering through one of the first-order haloes (A_{12}, A_{23}), gives an irradiance distribution at the observation plane as

$$\begin{aligned}\mathscr{I}_{(A_{12},A_{23})} = C[4 &+ 2\cos(\phi_{23} - \phi_{12}) + 2\cos(\phi_{23} - \phi_{12} + \delta_{23}) \\ &+ 2\cos(\phi_{23} - \phi_{12} - \delta_{12}) + 2\cos(\phi_{23} - \phi_{12} + \delta_{23} - \delta_{12}) \\ &+ 2\cos(\delta_{12}) + 2\cos(\delta_{23})]\end{aligned} \tag{7}$$

where C is a constant.

All the terms containing ϕs are random and contribute to speckle noise. The last two terms in the equation contribute to fringe formation.

Similarly filtering via the second-order halo A_{13} yields the irradiance distribution in the image as

$$\mathscr{I}_{(A_{13})} = C'[1 + \cos\delta_{13}] \tag{8}$$

In order to understand the formation of various kinds of fringe patterns, we present explicit expressions for the phase differences δ_{12}, δ_{23} and δ_{13}, introduced by deformation. These can be derived from eqn (4) and are given below

$$\begin{aligned}\delta_{12} &= \delta_1 - \delta_2 = (\mathbf{K}_4 - \mathbf{K}_1)\,.\,(\partial\mathbf{L}/\partial x)\Delta x_o + (\mathbf{K}_4 - \mathbf{K}_3)\,.\,\mathbf{L}(x, y) \\ \delta_{23} &= \delta_2 - \delta_3 = (\mathbf{K}_3 - \mathbf{K}_2)\,.\,\mathbf{L}(x, y) \\ \delta_{13} &= \delta_1 - \delta_3 = (\mathbf{K}_4 - \mathbf{K}_1)\,.\,(\partial\mathbf{L}/\partial x)\Delta x_o + (\mathbf{K}_4 - \mathbf{K}_2)\,.\,\mathbf{L}(x, y)\end{aligned} \tag{9}$$

Assuming that all the propagation vectors $\mathbf{K}_1$, $\mathbf{K}_2$, $\mathbf{K}_3$ and $\mathbf{K}_4$ lie in the x–z plane, and that the angles made by aperture separation at the object plane are very small, we obtain

$$\begin{aligned}\delta_{12} &= \frac{2\pi}{\lambda}\left[\frac{\partial u}{\partial x}(\sin\theta + \sin\alpha) + \frac{\partial w}{\partial x}(1 + \cos\theta)\right]\Delta x_o + \frac{2\pi}{\lambda}u\sin\alpha \\ \delta_{23} &= \frac{2\pi}{\lambda}u\sin\alpha \\ \delta_{13} &= \frac{2\pi}{\lambda}\left[\frac{\partial u}{\partial x}(\sin\theta + \sin\alpha) + \frac{\partial w}{\partial x}(1 + \cos\theta)\right]\Delta x_o + \frac{2\pi}{\lambda}2u\sin\alpha\end{aligned} \tag{10}$$

where θ_1, α are defined in Fig. 1. Under normal illumination ($\theta = 0$), these expressions reduce to

$$\delta_{12} = \frac{2\pi}{\lambda}\left[\frac{\partial u}{\partial x}\sin\alpha + 2\frac{\partial w}{\partial x}\right]\Delta x_o + \frac{2\pi}{\lambda} u \sin\alpha$$

$$\delta_{23} = \frac{2\pi}{\lambda} u \sin\alpha \tag{11}$$

$$\delta_{13} = \frac{2\pi}{\lambda}\left[\frac{\partial u}{\partial x}\sin\alpha + 2\frac{\partial w}{\partial x}\right]\Delta x_o + \frac{2\pi}{\lambda} 2u \sin\alpha$$

When the filtering is done via any one of the first-order haloes (A_{12}, A_{23}), the fringe patterns are formed corresponding to the phases δ_{12} and δ_{23}. The bright fringes are formed when

$$\left[\frac{\mathrm{d}u}{\mathrm{d}x}\sin\alpha + 2\frac{\mathrm{d}w}{\mathrm{d}x}\right]\Delta x_o + u \sin\alpha = m_1\lambda \tag{12}$$

$$u \sin\alpha = m_2\lambda \tag{13}$$

where m_1 and m_2 are integers.

Equation (12) represents a fringe pattern due to slope + strain + in-plane displacement components, while eqn (13) gives the fringe patterns due to the in-plane displacement component only. The in-plane displacement contribution to the derivative fringes is the same as that of the information obtained from eqn (13). This results in an overlapped pattern generated from the individual eqns (12) and (13).

When filtering is done via the second-order halo (A_{13}), the fringes are due to the phase term δ_{13}. The bright fringes are formed when

$$\left[\frac{\mathrm{d}u}{\mathrm{d}x}\sin\alpha + 2\frac{\mathrm{d}w}{\mathrm{d}x}\right]\Delta x_o + 2u \sin\alpha = m_3\lambda \tag{14}$$

Here the influence of in-plane displacement on the derivative fringes is twice as large as in eqn (12). In principle it is possible to obtain u, $\mathrm{d}u/\mathrm{d}x$ and $\mathrm{d}w/\mathrm{d}x$ from eqns (12)–(14). Since the angle α is very small, and the strain contribution is usually smaller than that of the slope, large errors are expected in the separation of these components. It may, however, be possible to neglect $(\mathrm{d}u/\mathrm{d}x)\sin\alpha$ in comparison to $2(\mathrm{d}w/\mathrm{d}x)$ in many experimental situations. Then the above equations reduce to

$$2(\mathrm{d}w/\mathrm{d}x)\Delta x_o + u \sin\alpha = m_1\lambda \tag{15}$$

$$u \sin\alpha = m_2\lambda \tag{16}$$

$$2(\mathrm{d}w/\mathrm{d}x)\Delta x_o + 2u \sin\alpha = m_3\lambda \tag{17}$$

It is interesting to note that in the absence of in-plane displacement, the fringe patterns obtained by filtering via first- and second-order diffraction haloes are identical and represent the partial slope change due to deformation. This is due to the fact that the sensitivity for the measurement of slope depends only on the amount of shear (Δx_o) and not on the apertures separation.[1] When the shear $\Delta x_o = 0$, the configuration is sensitive to the in-plane displacement component only.

3 SYMMETRICAL THREE-APERTURE CONFIGURATION WITH A SHEAR ELEMENT ON APERTURE A_2

The optical arrangement is the same as shown in Fig. 1 except that the shearing element (wedge plate) in the present arrangement is introduced in front of the aperture A_2 instead of aperture A_1. Two exposures are made, one before and one after loading. The irradiance distribution on the image plane for the first and second exposures are the same as given by eqns (1) and (2). However the phases δ_1, δ_2 and δ_3 are different. These are given by

$$\begin{aligned} \delta_1 &= (\mathbf{K}_4 - \mathbf{K}_1) \cdot \mathbf{L}(x, y) \\ \delta_2 &= (\mathbf{K}_3 - \mathbf{K}_1) \cdot \mathbf{L}(x + \Delta x_o, y) \\ \delta_3 &= (\mathbf{K}_2 - \mathbf{K}_1) \,.\, \mathbf{L}(x, y) \end{aligned} \tag{18}$$

The corresponding phase differences δ_{12}, δ_{23} and δ_{13} based on eqn (18) can be expressed as

$$\begin{aligned} \delta_{12} &= -(\mathbf{K}_3 - \mathbf{K}_1) \,.\, (\partial \mathbf{L}/\partial x)\Delta x_o + (\mathbf{K}_4 - \mathbf{K}_3) \,.\, \mathbf{L}(x, y) \\ \delta_{23} &= (\mathbf{K}_3 - \mathbf{K}_1) \,.\, (\partial \mathbf{L}/\partial x)\Delta x_o + (\mathbf{K}_3 - \mathbf{K}_2) \,.\, \mathbf{L}(x, y) \\ \delta_{13} &= (\mathbf{K}_4 - \mathbf{K}_2) \,.\, \mathbf{L}(x, y) \end{aligned} \tag{19}$$

The double exposure specklegram is placed in the whole-field filtering set-up as shown in Fig. 2. By filtering through the first- and second-order

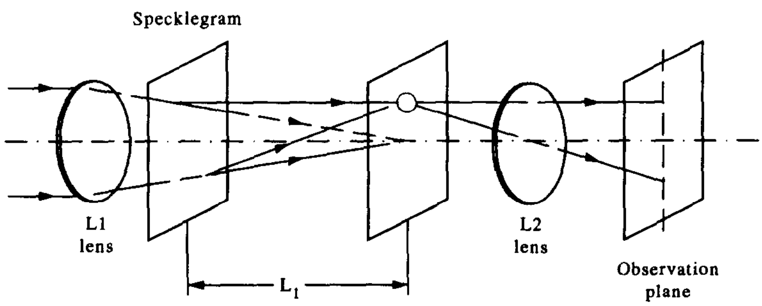

Fig. 2. Schematic of a whole-field filtering arrangement.

diffraction haloes (A_{12}, A_{23}), and A_{13}, as discussed in Section 2, two types of fringe patterns are obtained. Bright fringes are formed when

$$\delta_{12} = \frac{-2\pi}{\lambda}\left[\frac{\partial u}{\partial x}\sin\theta + \frac{\partial w}{\partial x}(1+\cos\theta)\right]\Delta x_o + \frac{2\pi}{\lambda}u\sin\alpha = 2m_1'\pi$$

$$\delta_{23} = \frac{2\pi}{\lambda}\left[\frac{\partial u}{\partial x}\sin\theta + \frac{\partial w}{\partial x}(1+\cos\theta)\right]\Delta x_o + \frac{2\pi}{\lambda}u\sin\alpha = 2m_2\pi \tag{20}$$

$$\delta_{13} = \frac{2\pi}{\lambda}2u\sin\alpha = 2m_3\pi$$

Under normal illumination ($\theta = 0$), eqn (20) reduces to

$$2(\mathrm{d}w/\mathrm{d}x)\Delta x_o - u\sin\alpha = m_1\lambda; \qquad m_1 = -m_1' \tag{21}$$

$$2(\mathrm{d}w/\mathrm{d}x)\Delta x_o + u\sin\alpha = m_2\lambda \tag{22}$$

$$2u\sin\alpha = m_3\lambda \tag{23}$$

These equations can be compared with those obtained in the earlier arrangement where the shear element is located on aperture A_1. Here, eqns (21) and (22) are independent of the strain term. It is obvious that there is no strain contribution to the fringe formation when the shear element is placed on the central aperture which is along the optical axis. The combined fringe pattern obtained from the first-order halo (A_{12}, A_{23}) contains information pertaining to the slope minus in-plane displacement contribution, and slope plus in-plane displacement contribution, while the second-order halo A_{13} contains the information pertaining to the in-plane displacement component only. The in-plane contribution in one case is subtracted [eqn (21)], while in another case it is added [eqn (22)]. The in-plane contributions, in both these cases are identical and its value is half of the value obtained from the halo A_{13} [eqn (23)]. A beat between these two sets of fringe patterns results in a moiré pattern similar to additive moiré. The moiré can be expressed as

$$2u\sin\alpha = (m_2 - m_1)\lambda = m_3\lambda \tag{24}$$

The fringe spacing of the beat moiré pattern is $\lambda/2\sin\alpha$. The in-plane displacement contribution is the same as that of the information obtained from halo A_{13}. In the absence of in-plane displacement, the resultant fringe pattern represents a good contrast slope pattern. When the shear $\Delta x_o = 0$, eqns (21) and (22) reduce to

$$u\sin\alpha = m\lambda \tag{25}$$

The fringe spacing is $\lambda/\sin\alpha$. So the in-plane displacement component obtained from the halo (A_{12}, A_{23}) will have half the sensitivity as that obtained from halo A_{13}.

4 EXPERIMENTAL RESULTS

The experiments are conducted on a centrally loaded diaphragm with its edge rigidly clamped using both configurations. The diaphragm is fabricated from a phosphor–bronze sheet of 0·7 mm thickness and 60 mm diameter. It is coated with an aluminium paint. The object is simultaneously subjected to both in-plane rotation and out-of-plane deflection. In the present experiment the influence of strain contribution on the object is absent. For in-plane motion the diaphragm is fixed on a precision rotation stage, while for the out-of-plane deflection, a micrometre head is provided at the centre of the diaphragm. The specimen is illuminated normally with collimated light from a 10 mW He-Ne laser. The aperture mask in front of the lens contains three 5 mm diameter holes with an interspacing of 20 mm. In the first experiment, a wedge plate with 1° wedge angle is mounted in front of the aperture A_1 (Fig. 1). The symmetrical three-aperture screen is properly mounted in front of a standard imaging lens ($f = 300$ mm). Two exposures, one before and the second after loading the object, are made on 10E75 holographic plate. The specimen is given about 5 μm central deflection and an in-plane rotation of about 3 milliradians. The filtering of double exposure specklegram is done on a Fourier filtering set-up (Fig. 2). The filtered fringe patterns via haloes (A_{12}, A_{23}) and A_{13} are shown in Fig. 3(a) and (b), respectively. The combined pattern in Fig. 3(a) results from the overlap of fringe patterns generated from individual eqns (15) and (16). One pattern represents in-plane displacement component, while the other is a modified slope pattern due to the influence of the in-plane displacement component. In Fig. 3(b) the influence of in-plane displacement on slope pattern is twice as large as in Fig. 3(a): evidently the slope fringes are more distorted.

In the second experiment, the wedge plate is mounted in front of aperture A_2. Two exposures are made on a holographic plate keeping the experimental parameters and loading the same as described above. Figure 4(a) and (b) shows the combined patterns and the in-plane displacement component pattern when the filtering is done via halo (A_{12}, A_{23}) and halo A_{13}, respectively. The combined pattern in Fig. 4(a) results from the overlap of fringe patterns generated from individual eqns (21) and (22). This results in a beat moiré which can be seen as discontinuities in the photograph. The lines joining these discontinuities represent the in-plane contribution which is the same as that obtained from halo A_{13}. This

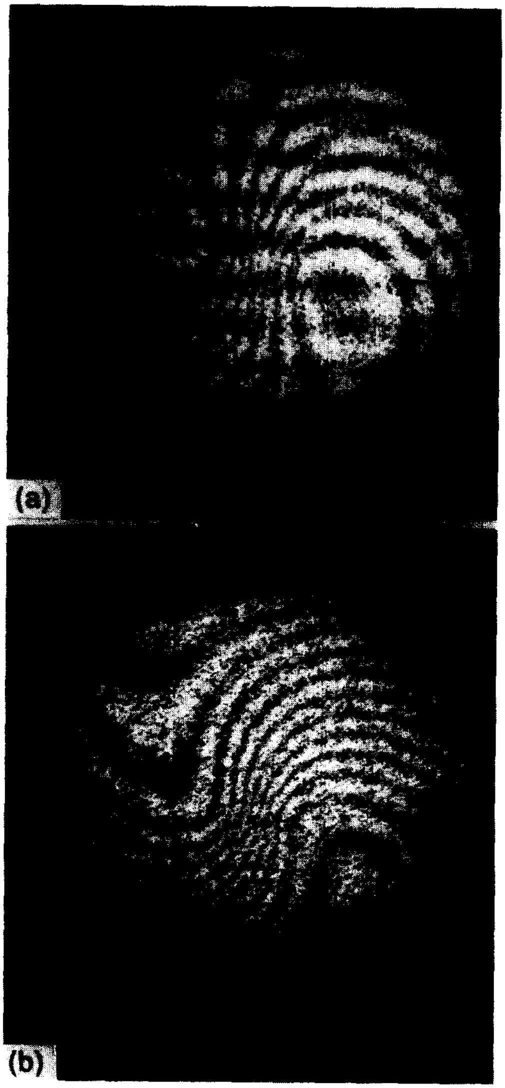

Fig. 3. (a) Combined fringe patterns filtered via halo (A_{12}, A_{23}). The fringes resulted due to overlap of two individual patterns. (b) Modified slope pattern with twice the sensitivity of in-plane displacement contribution.

analysis clearly shows that the influence of the in-plane displacement contribution can markedly modify the slope pattern and further the location of a shearing element in the aperture configuration plays an additional role in fringe formation.

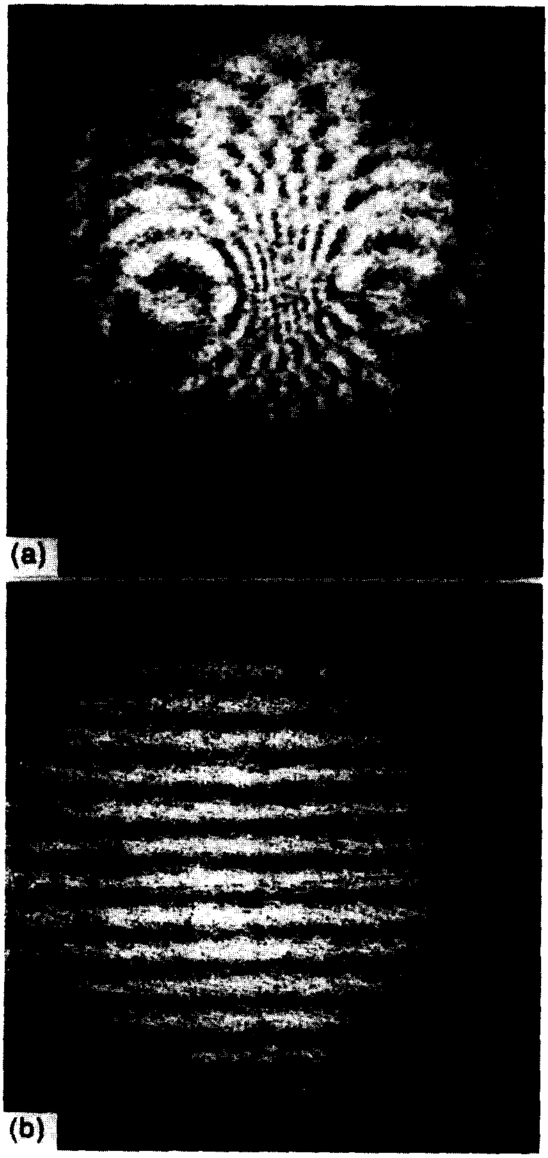

Fig. 4. (a) Overlapped fringe patterns filtered via halo (A_{12}, A_{23}) and (b) u component of in-plane displacement fringes filtered via halo A_{13}.

5 CONCLUSION

A study on fringe formation in a symmetrical three-aperture speckle shear interferometry is presented in this paper. It is also shown that the location of the shearing element in the aperture configuration plays an important role in fringe formation especially in the presence of in-plane displacement.

REFERENCES

1. Sirohi, R. S. (ed.), *Speckle Metrology*. Marcel Dekker, New York, 1993.
2. Shakher, C., Pramila Daniel, A. J. & Nirala, A. K., Temperature profile measurement of axisymmetric gaseous flames using speckle photography, speckle shear interferometry, and Talbot interferometry. *Opt. Engng*, **33** (1994) 1983–8.
3. Hung, Y. Y. & Liang, C. Y., Image shearing camera for direct measurement of surface strains. *Appl. Opt.*, **18** (1979) 1046–51.
4. Sirohi, R. S., Speckle shear interferometry—a review. *J. Opt.* (*India*), **13** (1984) 95–113.
5. Sirohi, R. S., Speckle shear interferometry. *Opt. Laser Technol.*, **16** (1984) 251–5.
6. Brdicko, J., Olson, M. D. & Hazell, C. R., Theory for surface displacement and strain measurements by laser speckle interferometry. *Opt. Acta*, **25** (1978) 963–89.
7. Brdicko, J., Olson, M. D. & Hazell, C. R., New aspects of surface displacement and strain analysis by speckle interferometry. *Exp. Mech.*, **19** (1979) 160–5.
8. Iwahashi, Y., Iwata, K. & Nagata, R., Influence of in-plane displacement in single aperture and double aperture speckle shear interferometry. *Appl. Opt.*, **24** (1985) 2189–92.
9. Krishna Mohan, N., Masalkar, P. J., Murukeshan, V. M. & Sirohi, R. S., Separation of the influence of in-plane displacement in multiaperture speckle shear interferometry. *Opt. Engng*, **33** (1994) 1973–82.